# Measurement of frequency gaps and waveguiding in phononic plates with periodic stepped cylinders using pulsed laser generated ultrasound

Jin-Chen Hsu, Tsung-Tsong Wu, and Hua-Shien Hsu

Citation: Journal of Applied Physics **113**, 083511 (2013); doi: 10.1063/1.4793491
View online: http://dx.doi.org/10.1063/1.4793491
View Table of Contents: http://scitation.aip.org/content/aip/journal/jap/113/8?ver=pdfcov
Published by the AIP Publishing

# Measurement of frequency gaps and waveguiding in phononic plates with periodic stepped cylinders using pulsed laser generated ultrasound

Jin-Chen Hsu,[1,a)] Tsung-Tsong Wu,[2] and Hua-Shien Hsu[1]
[1]*Department of Mechanical Engineering, National Yunlin University of Science and Technology, Douliou, Yunlin 64002, Taiwan*
[2]*Institute of Applied Mechanics, National Taiwan University, Taipei, Taiwan 106, Taiwan*

(Received 29 November 2012; accepted 11 February 2013; published online 25 February 2013)

In this paper, we theoretically and experimentally study phononic band gaps and waveguiding for plate-mode acoustic waves in a square array of stepped cylinders coated on an aluminum thin plate. We show that the stepped cylinders shaped with a small segment of reduced diameter can change the phonon resonance frequencies and result in tailorable band gaps. We demonstrate the band-gap and waveguiding effects in the phononic plate utilizing finite-element method numerical calculations and pulse laser ultrasonic measurements. Experimental results agree well with the numerical predictions. The phononic band gaps, slow resonant acoustic waves, and waveguiding in the lower frequency range are experimentally observed. The results enable enhanced control over phononic metamaterial, which has applications in low-frequency guiding and isolation of acoustic waves, acoustic absorbers, and nondestructive evaluation. © *2013 American Institute of Physics*. [http://dx.doi.org/10.1063/1.4793491]

## I. INTRODUCTION

Phononic crystals are artificial elastic structures that modulate periodically their acoustic properties in real space according to specific lattice symmetries.[1–3] The physical analogy between light and acoustic waves has attracted great interest in studying the scattering behaviors of acoustic waves in the periodic elastic structures because of the possibilities giving rise to frequency forbidden bands (i.e., band gaps) and maneuverable acoustic band structures for full control of wave propagation.[4–6] Phononic structures of two- and three-dimensional (2D and 3D) periodicities exhibit fully planar and spatial stoppage of acoustic wave propagation in any direction, which can be used to construct high-efficiency 2D and 3D acoustic waveguides and to develop frequency filters and acoustic-wave resonators.[7–9] Frequency forbidden bands were also utilized to build acoustic resonance cavities to launch a highly amplified narrow-band elastic energy flow based on the phonon tunneling through phononic finite lattices.[10,11] The acoustic band structures have also shown extraordinary characteristics that allow controlled propagation, such as slowing wave velocities, collimation, negative refraction, and perfect focusing.[12–15]

Typical phononic crystals are heterogeneous media constituted by periodic arrays of inclusions embedded in a matrix. The band gaps result from a large contrast in the value of the elastic stiffness and/or the mass density of the constitutive materials. Since acoustic waves in solids can propagate with the forms of longitudinal and transverse polarizations, wave scattering in heterogeneous media like phononic crystals causes the mixed polarization modes. This phenomenon found that no counterpart in light waves leads to phononic crystals to generate controlled energy conversions.[16–18] Phononic crystal investigations have been extended to surface waves and plate waves for highly planar confined propagation of acoustic waves using a free surface boundary parallel to the periodic planes.[19–23] The free-surface boundary confinement has further triggered the study of phononic crystals constituted by single material. Conventional homogeneous phononic crystal structures are made by etching a periodic air-hole array in a homogeneous matrix, where multiple scattering induced band gaps were found.[24–26] Recently, band gaps and band structures in 2D arrays of spheres or cylinders coated on surfaces of a half space and a plate of finite thickness were studied.[27–31] These spheres and cylinders arrays can be made of the material the same as or different from the half space (or the plate) to form the homogeneous or heterogeneous phononic structures. These coated scatterers (i.e., the spheres and cylinders) cause not only multiple scattering of acoustic waves but also resonances of themselves, while the acoustic waves are trapped in the scatterers by the surrounding free surface boundaries, analogous to Bragg scattering and Mie resonances in periodic elastic composite of embedded scatterers, respectively, and open absolute band gaps due to the scattering and resonance mechanisms in the reverent wavelengths. The method of using coating scatterers exterior to a half space or a plate can generate more tunable parameters for acoustic band structures.

In this paper, we study plate waves in a square array of stepped cylinders coated on a thin plate of the same material to form a homogeneous phononic-crystal plate. We show that the stepped cylinders shaped with a small segment (or a neck) of reduced diameter can change the resonance frequencies and result in tailorable band gaps. These effects are achieved by generating tunable scattering factor (areas covered by the cylinders on the thin plate) and structural stiffness by reducing the neck diameter. We further investigate experimentally the band-gap and guiding effects in the square-lattice stepped cylinders phononic plate using pulsed laser generated ultrasound, and report on the observation of

[a)]E-mail: hsujc@yuntech.edu.tw.

 

absolute band gaps, slow-wave resonances in stepped cylinders, and propagation of defect modes in the band gaps that are introduced by removing successive cylinders from a perfect square lattice. The measured results are discussed and compared with the theoretical calculations of the acoustic band structure and spectra.

This paper is organized as follows. Section II describes the phononic plate structure geometry and the computational and experimental methods. Section III presents and discusses the analysis and measured results of band gaps, resonances, and waveguiding effect in the phononic plate, respectively. Finally, Sec. IV concludes this study.

## II. STRUCTURE AND METHODS

The phononic structure presented here is a 2D array of stepped cylinders arranged in accordance with the square lattice with a lattice spacing $a$ coated on a thin plate of thickness $e$. The stepped cylinders have a head of diameter $d_1$ and length $h_1$, and a neck of reduced diameter $d_2$ and small length $h_2$. Figure 1(a) shows the schematics of the unit cell and the phononic plate structure. We define a reduced packing factor $F_r = \pi d_2^2/4a^2$, as the total area on the plate surface covered by the neck of the stepped cylinders. Figure 1(b) illustrates the irreducible first Brillouin zone of square lattice for wave propagation. Acoustic waves propagating in a thin plate are subjected to the constraint by the parallel free surfaces so that their wave numbers along the thickness are discrete and infinite plate modes forms (known as the A$n$, S$n$, and SH$n$ modes, $n = 0, 1, 2, \ldots$). These plate modes are dispersive while their eigenfrequencies are dependent on both the wave numbers along the plate thickness and along the propagation direction. The stepped cylinders introduced on the thin plate serve as local resonators to trap plate wave energy of frequency relevant to the characteristic resonance length and effective mass and stiffness of the cylinders. The behaviors expected to observe are localized cylinder resonances and slowing/stopping of the plate wave propagation. The reduced neck diameter of the stepped cylinders can accordingly modulate the resonances for tailoring the bandgap and guiding frequency range in phononic plates.

We manufactured the 2D phononic plates with a square-lattice array of stepped cylinders for the experimental measurement as shown in Figs. 1(c)–1(e). The phononic plates are homogeneous and constituted by aluminum (Al 6016). The experimental setup of pulsed laser measurements is sketched in Fig. 2. The wide-band ultrasonic waves were generated in the phononic plate by a nanosecond pulsed laser beam (Nd:YAG pulsed laser, 10-ns pulse duration) focused onto the plate surface. The transmitting signals were received by conical piezoelectric transducers, post amplified, and digitized by a digital oscilloscope with a 20-MHz sampling rate. Fast Fourier transformation (FFT) was used to obtain the spectra of the measured signals. The system was first calibrated with a bare thin plate of thickness the same as $e$ with no stepped cylinders to obtain a reference signal to normalize the subsequent spectra. The conical piezoelectric transducers suited to longitudinal and transverse vibrations of the waves were applied for the signal detection, respectively. When the constitutive materials of phononic structures are all isotropic (e.g., Al), the material properties do not break the original lattice symmetry, and the absolute band gaps can be identified experimentally, in principle, from the spectra measured along the two highest symmetry directions, i.e., the $\Gamma X$ and $\Gamma M$ directions, of the first Brillouin zone, respectively.

Finite element method (FEM) with eigenfrequency analysis was used to compute the acoustic band structures of the phononic plate. According to Newton's second law, elastic waves in a lossless medium are governed by the following equation for the displacement field $u_i$:

$$\rho \frac{\partial^2 u_i}{\partial t^2} - \frac{\partial}{\partial x_j}\left(c_{ijkl}\frac{\partial u_k}{\partial x_l}\right) = F_i, \qquad (i,j,k,l = x,y,z), \quad (1)$$

where $F_i$ denotes the body force, $\rho$ is the mass density, and $c_{ijkl}$ are the elastic stiffness constants. $x_i$ and $t$ in the equation are the coordinate and time variables, respectively. In the eigenfrequency analysis, the force term is absent, and a time-harmonic wave solution, $u_i(x, y, z, t) = u_i(x, y, z)e^{i\omega t}$, is assumed, where $\omega = 2\pi f$ is the angular frequency, $f$ denoting the frequency. In obtaining an acoustic band structure, the phononic plate was assumed to be periodic and infinite in extent in two dimensions ($x$ and $y$), where the unit cell of the

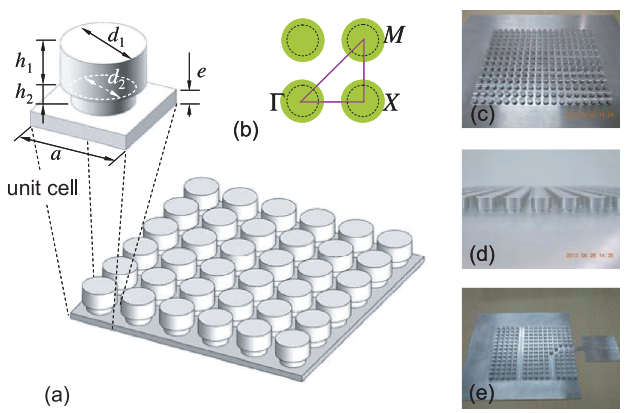


FIG. 1. (a) Phononic crystal consisting of stepped cylinders arranged in square lattice and coated on a thin plate. Enlarged plot shows the unit cell and dimensions. (b) Irreducible first Brillouin zone $\Gamma XM\Gamma$ of square lattice in wavevector space. (c) Top view and (d) side view of the manufactured phononic plate without defects. (e) Manufactured phononic plate with line defects to serve as straight and 90° bent waveguides.

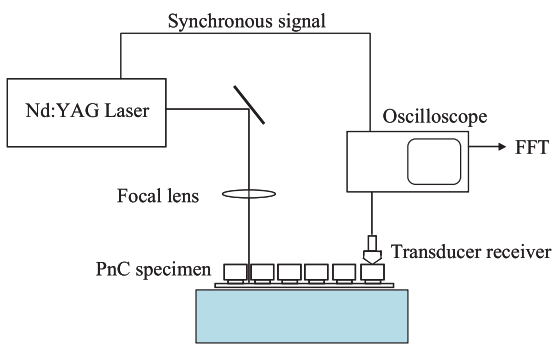


FIG. 2. Scheme of the experimental setup of laser ultrasonic measurement.

structure consists of a single stepped cylinder on a square plate of edge length $a$. In the unit cell, Bloch-Floquet periodic boundary conditions as follows were applied on the interfaces adjacent to the four neighboring unit cells

$$u_i(x + ma, y + na, z) = u_i(x, y, z)\exp(-ik_x ma - ik_y na), \quad (2)$$

where $k_x$ and $k_y$ are the $x$- and $y$-components of wavevector in the first Brillouin zone, respectively, and $m$ and $n$ are arbitrary integers. For the other surfaces of the unit cell surrounded by air, the following stress-free boundary conditions were applied:

$$(c_{ijkl}\,\partial u_k/\partial x_l)n_j = 0, \quad (3)$$

where $n_j$ is the unit vectors outward normal to the stress-free surfaces. This approach also obtains the eigenmodes associated with each point in the acoustic band structure on the frequency-wavevector domain. For the practical implementation of the FEM calculations, we used COMSOL MULTIPHYSICS software.[32] Frequency response analysis based on the FEM also provided us with the transmission calculations for monochromatic incident waves through finite lattice periods of phononic plate. The generation of a specific monochromatic incident plate wave mode with displacement $u_k$ on a surface was using a distributed sinusoidal surface force $f_i$, the relation is given by

$$(c_{ijkl}\,\partial u_k/\partial x_l)n_j = f_i. \quad (4)$$

The transmitted acoustic power flow $P$ can be calculated with the time-averaged surface integral of the Poynting vector of acoustic wave propagation, as

$$P = \frac{1}{T}\int_t^{t+T}\oint_S\left(-c_{ijkl}\frac{\partial u_k}{\partial x_l}\frac{\partial u_j}{\partial t}\right)n_i dS dt, \quad (5)$$

where $T$ is the time period of the monochromatic waves and $S$ is the wave transmitting cross-sectional area. Perfectly matched layers (PMLs) were utilized to absorb the incident radiation without producing reflection at the finite domain boundaries in the frequency response analysis. The analysis follows the procedure described in detail in Ref. 33, and further allows us to understand the incident plate mode influences on the transmission.

## III. RESULTS AND DISCUSSIONS

### A. Band gaps in phononic plates with periodic stepped cylinders

This subsection first demonstrates the effects of reduced neck diameter on the band gaps and acoustic band structure. Figure 3 shows the computational results of the band structure variation with gradually reducing the neck diameter $d_2$ to form the stepped cylinder from a uniform cylinder of diameter $d_1 = 7.5$ mm ($d_2 = d_1$). In the calculation for Fig. 3, the lattice spacing and plate thickness are $a = 10.0$ mm and $e = 1.0$ mm, respectively. The heights of the head cylinder and neck cylinder are $h_1 = 4.0$ and $h_2 = 1.0$ mm, respectively, corresponding to a fixed total height $h = h_1 + h_2 = 5.0$ mm of the stepped cylinders. The shaded frequency ranges in Fig. 3 denote the absolute band gaps. Therefore, below 200 kHz, this phononic plate can exhibit two obvious absolute band gaps that offer fully planar prohibition of wave propagation, while a third absolute band gap around 190 kHz in Fig. 3(c) is rather narrow that may not be efficient in stopping waves with a finite lattice. In the figures, the second absolute band gap is limited to its two edge frequencies at point $X$. As reducing the neck diameter, the lower edge frequency of the second absolute band gap remains unchanged, while the upper edge frequency is gradually decreasing. This causes gradual reduction of the second absolute band gap width. The mid-gap frequency and relative gap width (band-gap width over mid-gap frequency) are changed from 175.6 kHz and 21.9% to 161.8 kHz and 12.81%, respectively, as $d_2$ is reduced from 7.5 mm to 6.7 mm. For the first absolute band gap in a much lower frequency range, both its lower and upper edge frequencies are going down as the neck diameter is reducing. The mid-gap frequency and relative gap width are changed from 54 kHz and 20.4% (uniform cylinder, $d_2 = d_1$) to 40.1 kHz and 20.87% ($d_2 = 6.7$ mm), respectively. Table I lists the band-gap ranges and their relative gap widths for several neck diameters. Introducing a neck in the cylinders can be effective in tuning the band gaps when the gap edge frequencies are sensitive to the neck diameter.

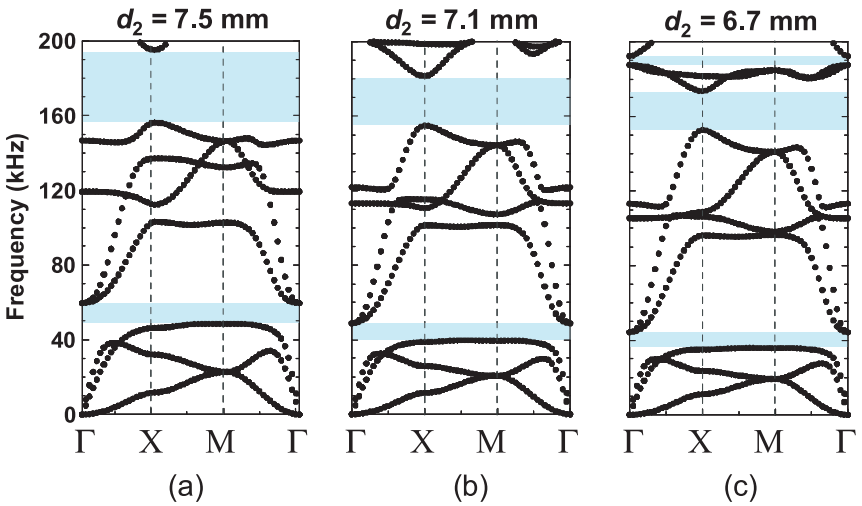


FIG. 3. Acoustic band structures of the square lattice phononic plate with periodic stepped cylinders of different neck diameters $d_2$. (a) $d_2 = 7.5$ mm (uniform cylinder), (b) $d_2 = 7.1$ mm, and (c) $d_2 = 6.7$ mm, where the lattice constant, plate thickness, head diameter, head length, and neck length are fixed at $a = 10.0$ mm, $e = 1.0$ mm, $d_1 = 7.5$ mm, $h_1 = 4.0$ mm, and $h_2 = 1.0$ mm, respectively.

TABLE I. Band-gap ranges and widths with different neck diameters. Geometry parameters: $a = 10.0$ mm, $e = 1.0$ mm, $d_1 = 7.5$ mm, $h_1 = 4.0$ mm, $h_2 = 1.0$ mm.

| Neck diameter $d_2$ (mm) | First absolute band gap (kHz) (Relative gap width) | Second absolute band gap (kHz) (Relative gap width) |
|---|---|---|
| 7.5 (=$d_1$) | 48.5–59.5 (20.40%) | 156–195.2 (21.90%) |
| 7.3 | 41.3–51.4 (21.50%) | 155.6–185.3 (16.99%) |
| 7.1 | 39.4–48.8 (21.26%) | 154.5–181.6 (15.68%) |
| 6.9 | 37.6–46.5 (20.92%) | 153.3–177.6 (14.24%) |
| 6.7 | 35.9–44.3 (20.87%) | 152–173.6 (12.81%) |

To understand the influences of the neck on power transmissions, Fig. 4 presents the calculated transmission spectra for incident plate waves to propagate through finite phononic plates of six periods. For comparison purpose, we consider the cases of uniform cylinders (i.e., $d_2 = d_1 = 7.5$ mm) and stepped cylinders of $d_2 = 6.7$ mm. Several different incident plate modes have been considered. Figures 4(a)–4(c) and 4(d)–4(f) are calculated transmission spectra corresponding to the incidence of the S0, SH0, and A0 plate modes from the thin plate in the $\Gamma X$ and $\Gamma M$ directions of square lattice, respectively. The dashed curves denote the case with the uniform cylinders, and the solid curves denote the case of stepped cylinders. Different plate modes incident to the phononic plates are considered because the transmission may be susceptible to the acoustic energy ratio converted into phononic plate eigenmodes from different incident plate modes. In Fig. 4, the spectra show well transmissible ranges and the spectral gaps with a transmission dip or trough. The ranges of the spectral gaps contain the absolute band gaps (the shaded ranges) shown in Fig. 3(c). The appearance of the spectral gap ranges associated with the absolute band gaps does not depend on the incident modes and propagation directions, while the extra spectral gap ranges are directional or incident-mode dependent. The incident-mode dependent spectral gaps can be regarded as being deaf to specific incident modes (or deaf bands) and can serve as mode selected band gaps. Comparing to the case of the uniform cylinders, the spectral gaps generally down shift to lower frequency ranges for the case of the stepped cylinders. Using the stepped cylinder array lowers not only the absolute band gaps but also the frequency ranges of deaf bands and directional band gaps. The frequency shift originates mainly from the modification of structural stiffness and effective mass of the cylinders with the neck. As a result, the frequency bands in the band structures are changed to lower frequencies, leading to the tailorable band gaps toward the lower frequency ranges. In Figs. 4(c) and 4(f), the transmission spectra using A0 mode incidence show a wide range of depressed transmission coefficients (about 20–30 dB reduction) in between the first and second absolute band gaps. This provides weaker forbiddance for the A0 mode propagation in that range than in the true absolute band gaps. As a result, wave energy propagation depression, shorter range waveguiding, and weaker confinement for A0 mode can be achieved in a wide frequency range in the phononic plates.

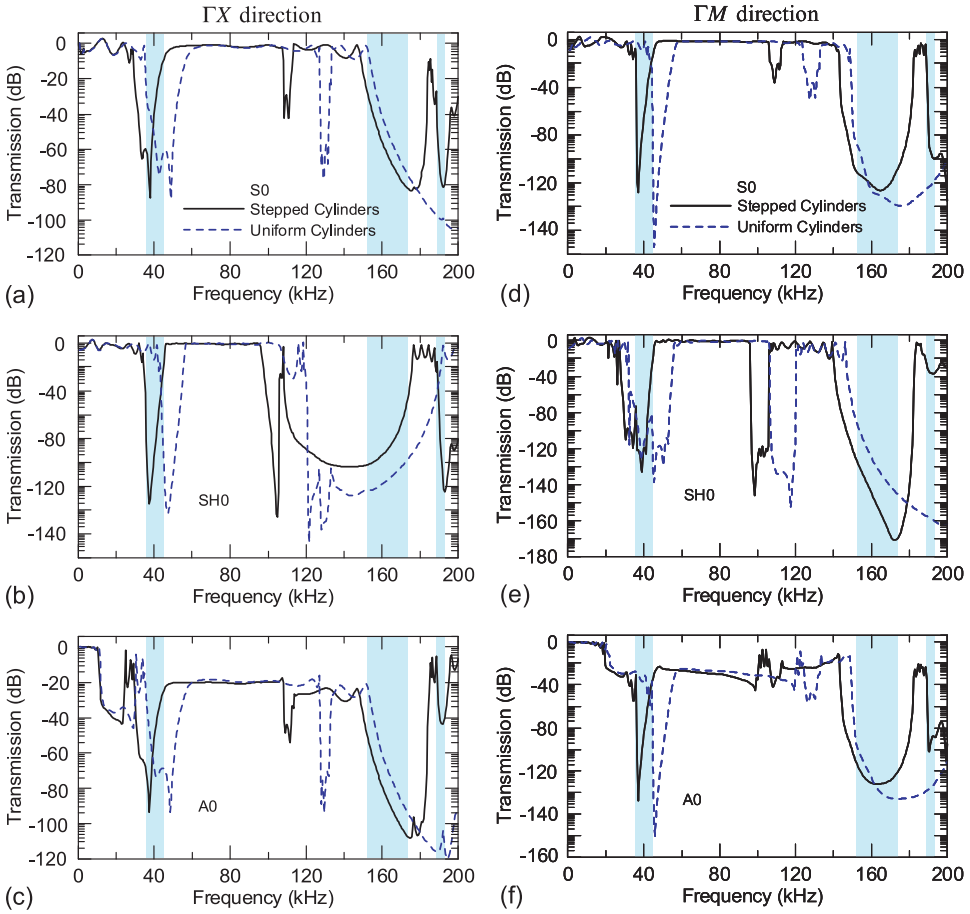


FIG. 4. Calculated transmission spectra of different plate modes incident into the finite phononic plates of six unit cells along $\Gamma X$ ((a)–(c)) and $\Gamma M$ ((d)–(f)) directions, respectively. The solid curves and dashed curves represent the case of stepped cylinders of neck diameter $d_2 = 6.7$ mm and the case of uniform cylinders of diameter $d_2 = d_1 = 7.5$ mm, respectively. (a)–(c) Incident waves are S0, SH0, and A0 plate modes along the $\Gamma X$ direction, respectively. (d)–(f) Incident waves are S0, SH0, and A0 plate modes along the $\Gamma M$ direction, respectively.

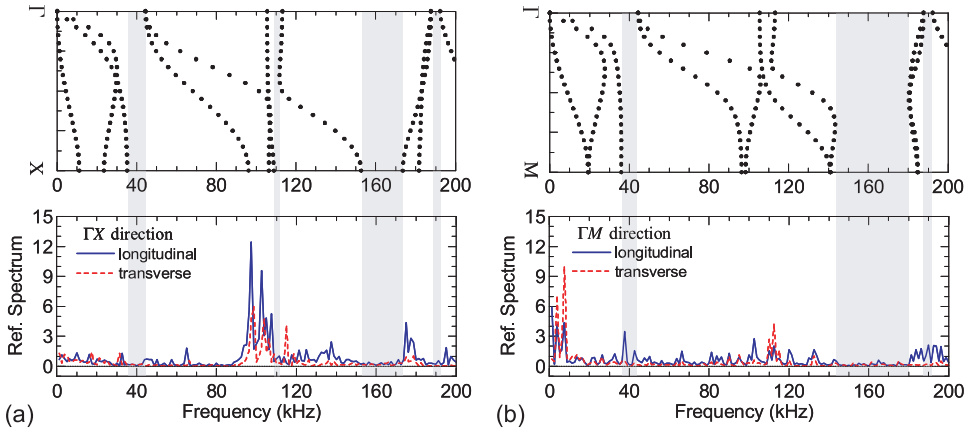


FIG. 5. Measured reference spectra for pulsed laser generated ultrasonic waves in the phononic plate propagating along the $\Gamma X$ (a) and $\Gamma M$ (b) directions, respectively. Solid and dashed curves represent the measurements using the longitudinal the transverse transducers, respectively. The transducers are located on the top surface of a stepped cylinder to receive the wave signals. Five stepped cylinders lie in between the pulsed laser source spot and the transducer receivers. The acoustic band structures of corresponding propagation directions are shown above for comparison. The frequency ranges marked as gray denote the band gaps along the direction.

### B. Laser ultrasonic characterization

For experimental characterization, we fabricated an array of stepped cylinders with a neck diameter $d_2 = 6.7$ mm on the thin plate of thickness $e = 1.0$ mm (Figs. 1(c) and 1(d)). This structure has a reduced packing factor $F_r = 0.352$ on the plate surface. The first two absolute band gaps range from 35.9 to 44.3 kHz and from 152 to 173.6 kHz. In the measurement, the pulsed laser beam was focused on the plate surface in the cylinder array and generated wide-band ultrasound in the plate, and conical transducers contacted the top surface of one stepped cylinder to receive the vibration signals. Five stepped cylinders lay in between the pulsed laser source spot and transducer receiver. The structure totally contains 16 rows and 18 columns of cylinders, and the Al thin plate has extended area out of the cylinder array area to delay the arrival of the out-going waves reflected by the plate edges. Absorbing material was also smeared on the extended plate surfaces to eliminate the reflection. Figures 5(a) and 5(b) show the measured results for the phononic plate structure along the $\Gamma X$ and $\Gamma M$ directions, respectively. All the measurements using the longitudinal and transverse transducers show low transmitting intensity in the band-gap ranges from 35.9 to 44.3 and 152 to 173.6 kHz in the spectra, and there have some obvious transmission drops around the band-gap edges that may be depending on the used transducer type. This shows the effect of the polarization difference among the gap-edge modes. In addition, it is also observed that several vibration peaks around 100 kHz are pronounced in the $\Gamma X$ and $\Gamma M$ directions. Around 100 kHz, there are curves in the acoustic band structure exhibiting small slopes, which correspond to the slow-down of the modes. As the slow modes are relevant to the resonances of the stepped cylinders, the signals measured on the cylinder top surfaces can then show outstanding peaks associated with the cylinder vibrations in the spectra. Therefore, these peaks are corresponding to the frequencies of the curves of small slopes or of the curves at the points on the Brillouin zone boundary.

### C. Straight and 90° bent line-defect waveguides

We consider the line-defect waveguide as shown in Fig. 1(e). Figure 6 shows the calculated defect bands in the absolute band gaps of the line-defect phononic plate. The results were obtained with the supercell approximation method, where the supercell contained nine unit cells. In the first absolute band gap (Fig. 6(a)), two defect bands stretch out into the band-gap range and are not overlapping in their frequencies. Therefore, pure mode guiding can be possible in the first absolute band gap. In the second absolute band gap (Fig. 6(b)), multiple defect bands exist and have overlapping frequencies, in which there can be different guided modes to propagate at the same frequency.

The total displacements and mode shapes of several defect modes are shown in Fig. 7. These modes are corresponding to the points *A*–*H* labeled in Fig. 6. Modes *A* and *B* are in the first absolute band gap, where mode *A* has a simple flexural vibration pattern and well confined to the waveguide, and mode *B* is not a well confined mode. Modes *C*–*H* are in the second absolute band gap and belong to different defect bands. Except mode *F* that is an extensional plate mode, the other modes are flexural mode with different out-of-plane mode shapes. The modes *D* and *E* have vibrations localized only in the thin plate of the waveguide, while the modes *C*, *F*, *G*, and *H* contain also obvious vibration of the stepped cylinders neighbor the waveguide. Since modes *C*, *F*, *G*, and *H* penetrate deeper into the cylinder array area, these modes can have easier coupling to acoustic energy outside waveguide by reducing isolation cylinder layers to one or two. The guided defect bands in the absolute band gaps

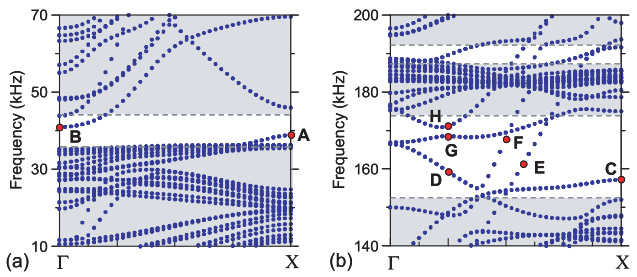


FIG. 6. Calculated defect bands of line-defect phononic plate with stepped cylinders in the absolute band gaps (the unshaded frequency ranges). One row of cylinders is assumed to be removed from the perfect stepped cylinder array to form the line defect. (a) Defect bands in the first absolute band gap; (b) defect bands in the second and third absolute band gaps. The results are obtained using the supercell approximation method with nine unit cells contained.

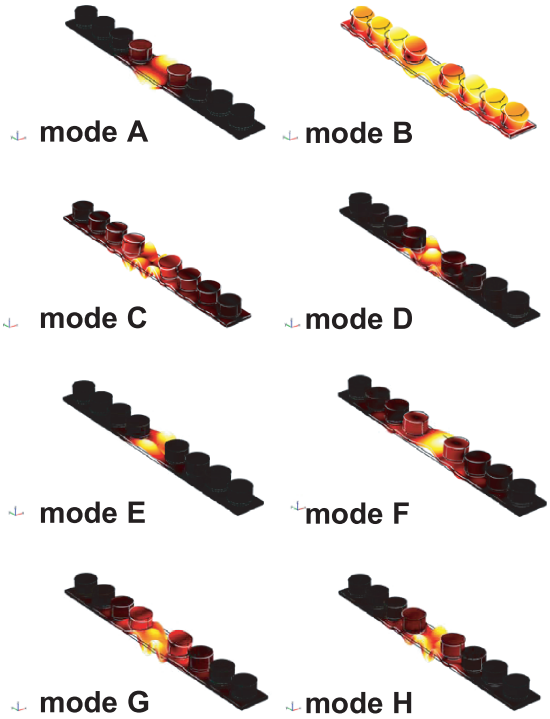


FIG. 7. Total displacement fields and mode shapes of several line-defect modes in the first and second absolute band gaps. The frequencies of modes *A*–*H* are correspondingly labeled in Fig. 6. Modes *A* and *B* belong to the two defect bands in the first absolute band gap, where only mode *A* is well confined to the line-defect waveguide. Modes *C*–*H* belong to the defect bands in the second absolute band gap. All the modes are well confined by the line-defect waveguide, where mode *F* is an extensional plate mode, and the other modes are flexural modes.

can be confined by the line defect along any direction on the *x*-*y* plane.

Figure 8 shows the measured reference spectra of the line defect waveguiding structure using the laser ultrasonic method presented in Subsection III B. The frequency ranges marked as gray in the figure cover the theoretical directional (in the $\Gamma X$ direction) and absolute band gaps. The conical transducer receivers were located in the line defect and contact the thin plate surface. The measurements were obtained with the longitudinal and transverse transducers, and the distance between the pulsed laser source spot and transducer receiver is $7a = 70$ mm. In the figure, both the longitudinal and transverse signals exhibit outstanding peaks and higher intensities in the second absolute band gap, which correspond to the fact that the injected energy is confined to propagate along the line defect in the frequency range. In the first band gap, two outstanding peaks are observed (the higher one is labeled as peak **a**). This agrees with the numerical result that there are defect bands with a small slope appearing in the first band gap. As shown in Fig. 7, the defect mode labeled as mode *A* is well confined to the waveguide with a single-cylinder removal width so that it should contribute to the peak **a** in Fig. 8 in the first band gap (though there is a small deviation between the calculated and experimental frequency values), while mode *B* leaks obvious acoustic energy into the cylinder array. The appearance of the other peak below the peak **a** is caused by the wider directional gap along the $\Gamma X$ direction, where flat extended defect bands exist on the gap edge. Outside the directional and absolute band gaps and between 44.3 and 152 kHz, inefficient mode conversion between the injected energy and phononic plate eigenmodes leads to non-vanishing intensity and peaks that are corresponding to the partial wave energy localization in the waveguide.

To understand further the wave propagation in the straight waveguide, FEM frequency response analysis was used to calculate the total displacement fields. We consider the responses at three peak frequencies labeled in Fig. 8 (peaks **a**, **b**, and **c**, corresponding to the frequencies 41.25, 156.25, and 103.75 kHz, respectively). Figure 9 shows the calculated results. In the calculation, a sinusoidal point source is applied at the middle of the line-defect waveguide, and PML is assumed outside the cylinder array area. Figure 9(a) is the calculated displacement field corresponding to the frequency at 41.25 kHz. This field has a simple displacement pattern similar to mode *A* and is confined around the waveguide. The displacement considerably penetrates into the first cylinder layer and decays along the waveguide. In Fig. 9(b) that corresponds to the higher frequency at 156.25 kHz, the calculated result shows that acoustic energy is better confined inside the waveguide to propagate and localized in the thin plate. As a result, the measured spectral intensity has

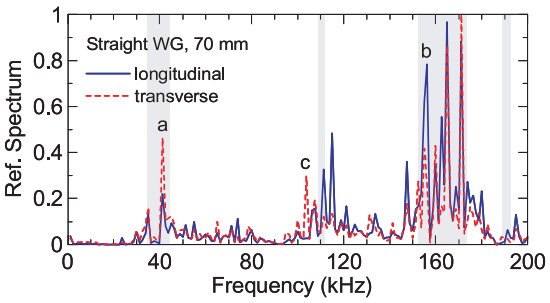


FIG. 8. Measured reference spectra of pulsed laser generated ultrasonic waves in the line-defect straight waveguide (Straight WG). The frequency ranges marked as gray denote the band gaps along the $\Gamma X$ direction. Solid and dashed curves represent the measurements using the longitudinal the transverse transducers, respectively. The laser source spot and the transducer receivers are in the waveguide and separated by $7a = 70$ mm along the guiding path.

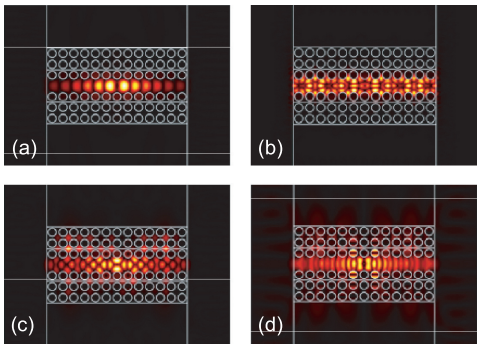


FIG. 9. Calculated frequency responses of total displacement intensity with a sinusoidal point source applied in the middle of the waveguide. (a) Frequency $f = 41.25$ kHz (in the first absolute band gap), (b) $f = 156.25$ kHz (in the second absolute band gap), and (c) $f = 103.75$ kHz (outside the absolute band gaps). (d) The same as (c) with only the *x*-component amplitude of the displacement field.

much higher values with frequencies in the second absolute band gap than that in the first absolute band gap. Experimental result in Fig. 8 shows also that, outside the band gaps, short range from the source in the waveguide is possible to preserve considerable acoustic energy by means of deaf bands or inefficient mode conversion. Figure 9(c) shows the calculated total displacement at the frequency 103.75 kHz. Though this frequency is outside the band gaps, the waves can still be weakly confined along the straight waveguide with considerable leaky energy into the cylinder array area. Figure 9(d) shows the $x$-component amplitude of the displacement field in Fig. 9(c). The field has also non-vanishing $x$-component amplitude, and the amplitude in the waveguide is larger than that of leaky waves.

Figure 10 shows the measured reference spectra for the bent line-defect waveguide. The signals were detected at points $R1$ and $R2$ (see the inset of Fig. 10(b)) in the bent waveguide, respectively. The signal at the entrance of the bent waveguide is used as the reference in obtaining Fig. 10. It can be observed that the intensity in the second absolute band gap is still pronounced, whereas the intensity in the first absolute band gap drops to very low values. In addition, in comparing Fig. 10(a) with 10(b), propagation loss is observed from the decayed intensity from point $R1$ to point $R2$. To explore the propagation of acoustic waves in the bent waveguide corresponding to the measured signals, several frequency responses of the total displacement fields were calculated and shown in Fig. 11. Figures 11(a)–11(e) are the calculated displacement fields with frequencies at 54, 70, 131 (outside the absolute band gaps), 161 (in the second absolute band gap), and 39 kHz (in the first absolute band gap), respectively, and the chosen frequencies are correspondingly indicated in Fig. 10 as points **d–h**. In Figs. 11(a)–11(c), the acoustic waves at 54, 70, and 131 kHz leak considerable energy into cylinder array area. However, partial acoustic energy can be guided by the waveguide for a short distance. These partially guided acoustic waves outside the absolute band gaps exhibit different behavior when meeting the bend. At 54 kHz, the waves in the waveguide cannot be bent and are reflected by the corner. The waves in the waveguide at 70 kHz can be bent but cannot transmit into the vertical route. For the waves at 131 kHz in the waveguide, transmission along the bent waveguide is achieved. In the second absolute band gap as shown in Fig. 11(d), the injected acoustic waves at 161 kHz transmit and well guided along the bent waveguide for a longer distance. The propagation loss is much less than those outside the band gap. An interesting observation in Fig. 11(d) is that conversion between two different guided modes (mode $D$ and mode $E$ in Fig. 7) occurs at the entrance and exit of the bent corner. This shows that multiple defect bands in the absolute band gap may benefit wave propagation in a bent waveguide by means of acoustic energy conversion among different defect modes to better adapt the corner shape. In the first absolute band gap as shown in Fig. 11(e), the injected acoustic waves at 39 kHz can propagate into the waveguide; however, the energy does not be bent to propagate forward. We conclude that the narrow path at the corner forbids the acoustic wave to propagate with such a low frequency, which is corresponding to a longer wavelength. As a result, transmission peak in the first absolute band gap was not experimentally observed in Fig. 10. Accordingly, we modified the corner of the bent waveguide by removing two more stepped cylinder scatterers at the corner and calculated the response of total displacement field at 39 kHz, as shown in Fig. 11(f). As a result of the modification, the low-frequency acoustic waves can be bent by the corner to propagate along the bent waveguide.

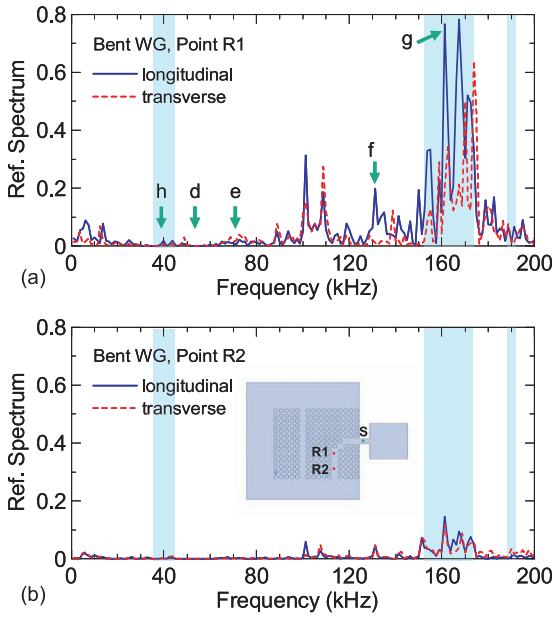


FIG. 10. Measured reference spectra of pulsed laser generated ultrasonic waves propagating in the 90° bent waveguide (Bent WG) at (a) point $R1$ and (b) point $R2$, respectively. The inset in (b) shows the locations of the laser source spot ($S$) and detection points ($R1$ and $R2$). The frequency ranges marked as gray denote the absolute band gaps. Solid and dashed curves represent the measurements using the longitudinal and transverse transducer receivers, respectively.

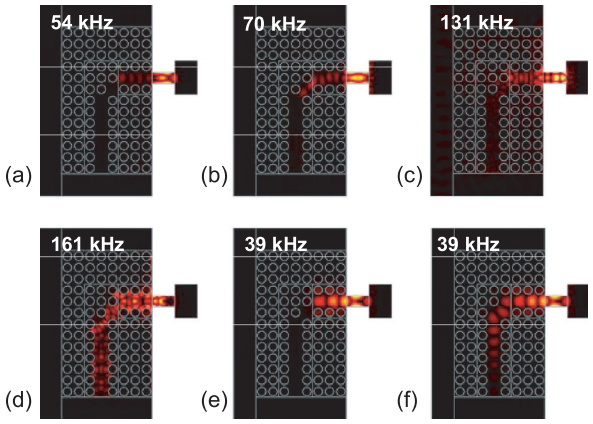


FIG. 11. Calculated frequency responses of total displacement intensity with a sinusoidal point source applied in the front of the 90° bent waveguide. (a)–(c) Frequencies $f = 54$, 70, and 131 kHz (in between the first and second absolute band gaps), (d) $f = 161$ kHz (in the second absolute band gap), and (e) $f = 39$ kHz (in the first absolute band gap). (f) The same as (e) with two more stepped cylinder scatterers being removed from the bending corner.

## IV. CONCLUSIONS

In conclusion, we have numerically and experimentally studied the band gaps, resonances, and waveguiding in

phononic structures composed of a stepped-cylinder array on a thin plate. We show that the band gaps can be effectively tuned by introducing the cylinders a small segment of different reduced diameters, which modified the effective structural stiffness and mass of the cylinders. By means of laser ultrasonic method, we measured the spectra for plate waves in the structure to determine the absolute band gaps and possible resonances in the stepped cylinders. The measured results agree well with the numerical results in the band gaps and slow resonant waves. Based on the numerical and experimental results of the band gaps, we showed the waveguiding effects for plate waves in the stepped-cylinder phononic crystal plate with straight and bent waveguides, respectively. Low and high frequency waveguiding effects were obtained and experimentally observed. In the higher (second) absolute band gap, waveguiding effect is pronounced in either the straight or bent waveguide. In the low-frequency absolute band gap, where the stepped-cylinder resonances contribute mainly to the band gap formation, waveguiding efficiency is sensitive to geometry at the corner of the bent waveguides because of the longer wavelength of low frequency waves in the thin plate area. As a result, well designed waveguide corner is required for low frequency waves. Applications include low-frequency guiding and isolation, acoustic absorbers, and nondestructive evaluation.

## ACKNOWLEDGMENTS

The authors gratefully thank the National Science Council of Taiwan for the financial support of this work (Grant Nos. NSC 100-2221-E-224-024 and NSC 101-2221-E-224-015).

[1]M. S. Kushwaha, P. Halevi, L. Dobrzynski, and B. Djafari-Rouhani, Phys. Rev. Lett. **71**, 2022 (1993).
[2]J. O. Vasseur, P. A. Deymier, A. Khelif, Ph. Lambin, B. Djafari-Rouhani, A. Akjouj, L. Dobrzynski, N. Fettouhi, and J. Zemmouri, Phys. Rev. E **65**, 056608 (2002).
[3]M. Sigalas and E. N. Economou, Solid State Commun. **86**, 141 (1993).
[4]A. Khelif, A. Choujaa, S. Benchabane, B. Djafari-Rouhani, and V. Laude, Appl. Phys. Lett. **84**, 4400 (2004).
[5]X. Zhang and Z. Liu, Appl. Phys. Lett. **85**, 341 (2004).
[6]I. E. Psarobas, N. Stefanou, and A. Modinos, Phys. Rev. B **62**, 5536 (2000).
[7]R. H. Olsson III and I. El-Kady, Meas. Sci. Technol. **20**, 012002 (2009).
[8]F.-C. Hsu, J.-C. Hsu, T.-C. Huang, C.-H. Wang, and P. Chang, Appl. Phys. Lett. **98**, 143505 (2011).
[9]S. Mohammadi, A. A. Eftekhar, W. D. Hunt, and A. Adibi, Appl. Phys. Lett. **94**, 051906 (2009).
[10]F.-C. Hsu, T.-T. Wu, J.-C. Hsu, and J.-H. Sun, Appl. Phys. Lett. **93**, 201904 (2008).
[11]S. Yang, J. H. Page, Z. Liu, M. L. Cowan, C. T. Chan, and P. Sheng, Phys. Rev. Lett. **88**, 104301 (2002).
[12]C.-Y. Sun, J.-C. Hsu, and T.-T. Wu, Appl. Phys. Lett. **97**, 031902 (2010).
[13]M. Ke, Z. Liu, C. Qiu, W. Wang, J. Shi, W. Wen, and P. Sheng, Phys. Rev. B **72**, 064306 (2005).
[14]S. Yang, J. H. Page, Z. Liu, M. L. Cowan, C. T. Chan, and P. Sheng, Phys. Rev. Lett. **93**, 024301 (2004).
[15]S.-C. S. Lin, T. J. Huang, J.-H. Sun, and T.-T. Wu, Phys. Rev. B **79**, 094302 (2009).
[16]B. Manzanares-Martínez and F. Ramos-Mendieta, Phys. Rev. B **76**, 134303 (2007).
[17]M. M. de Lima, Jr., P. V. Santos, Yu. A. Kosevich, and A. Cantarero, Appl. Phys. Lett. **100**, 261904 (2012).
[18]J.-C. Hsu, J. Phys. D: Appl. Phys. **46**, 015301 (2013).
[19]Y. Tanaka and S. Tamura, Phys. Rev. B **58**, 7958 (1998).
[20]T.-T. Wu, Z.-C. Hsu, and Z.-G. Huang, Phys. Rev. B **71**, 064303 (2005).
[21]J.-C. Hsu and T.-T. Wu, Phys. Rev. B **74**, 144303 (2006).
[22]A. Khelif, B. Aoubiza, S. Mohammadi, A. Adibi, and V. Laude, Phys. Rev. E **74**, 046610 (2006).
[23]J. O. Vasseur, P. A. Deymier, B. Djafari-Rouhani, Y. Pennec, and A-C. Hladky-Hennion, Phys. Rev. B **77**, 085415 (2008).
[24]S. Benchabane, A. Khelif, J.-Y. Rauch, L. Robert, and V. Laude, Phys. Rev. E **73**, 065601(R) (2006).
[25]T.-T. Wu, L.-C. Wu, and Z.-G. Huang, J. Appl. Phys. **97**, 094916 (2005).
[26]S. Mohammadi, A. A. Eftekhar, A. Khelif, W. D. Hunt, and A. Adibi, Appl. Phys. Lett. **92**, 221905 (2008).
[27]R. Sainidou and N. Stefanou, Phys. Rev. B **73**, 184301 (2006).
[28]T.-T. Wu, Z.-G. Huang, T.-C. Tsai, and T.-C. Wu, Appl. Phys. Lett. **93**, 111902 (2008).
[29]Y. Pennec, B. Djafari-Rouhani, H. Larabi, J. O. Vasseur, and A. C. Hladky-Hennion, Phys. Rev. B **78**, 104105 (2008).
[30]M. Oudich, M. B. Assouar, and Z. Hou, Appl. Phys. Lett. **97**, 193503 (2010).
[31]A. Khelif, Y. Achaoui, S. Benchabane, V. Laude, and B. Aoubiza, Phys. Rev. B **81**, 214303 (2010).
[32]COMSOL MULTIPHYSICS, COMSOL, Inc., see http://www.comsol.com.
[33]F.-C. Hsu, J.-C. Hsu, T.-C. Huang, C.-H. Wang, and P. Chang, J. Phys. D: Appl. Phys. **44**, 375101 (2011).